# Experimental study into tunnel face collapse in sand

J. Messerli, E. Pimentel & G. Anagnostou *ETH Zurich, Switzerland* 

ABSTRACT: We investigate the face failure mechanism for shallow circular tunnels that are excavated in a dry, cohesionless soil by means of a physical model and analyse the experimental results by means of limit equilibrium calculations. The physical model consists of a sand box with a tunnel, which was modelled by a clear acrylic half pipe. The tunnel face support was modelled in two ways: as a rigid movable face with a PVC plate; and as a flexible face with a pressurised air bag. A series of tests were performed with an overburden of one, two and three times the tunnel diameter. The kinematics of the failure body were determined, as well as the required support pressure. The test results agree well with the predictions of the analytical model.

#### 1 INTRODUCTION

The collapse of the face of a shallow tunnel may propagate towards the surface, thereby creating a crater and leading to third party damage. In order to assess the risk and to design appropriate countermeasures, it is essential to have reliable analyses of face stability and predictions of the necessary support pressure. The stability of the tunnel face is usually analyzed by limit equilibrium calculations and occasionally by numerical models (cf., e.g., Vermeer et al. 2002; Kirsch 2009).

Continuum-mechanical modelling provides predictions not only of the limit state but also of the development of deformations, while at the same time dealing with some of the uncertainties in limit equilibrium models caused by the presence of statically indeterminate forces in three-dimensional sliding mechanisms. On the other hand, modelling the deformational behaviour of the ground also introduces considerable uncertainties and this, in combination with the high computational effort required for three-dimensional analyses, limits the applicability of numerical modelling.

In tunnel engineering practice, the stability of the face is analyzed by means of limit equilibrium computations which mostly rely on the simple sliding mechanism proposed by Horn (1961). On account of the major practical importance of this computational method, an experimental investigation was carried out in order to re-evaluate the reliability of the model predictions (Messerli, 2007). The problem layout, together with an outline of the limit equilibrium model, the layout of the physical model and the results of this investigation will be presented in Sections 2, 3 and 4 of the present paper, respectively. Similar model tests have been carried-out recently by Vardoulakis et al. (2009)

and Kirsch (2009), while a comprehensive review of physical modelling of tunnels in soil can be found in Meguid et al. (2008).

#### 2 LIMIT EQUILIBRIUM ANALYSIS

We consider a shallow cylindrical tunnel of diameter D crossing a dry, cohesionless soil obeying the Coulomb yield criterion with the friction angle  $\phi$ . The depth of cover amounts to H (Figure 1). The tunnel wall is supported by a rigid lining up to a distance e behind the face (Figure 2). The force S that is needed in order to stabilize the face will be estimated by considering the limit equilibrium. The failure mechanism according to Horn (1961) approximates the circular face by means of a square and consists of a wedge and the overlying prismatic body (Figure 1). The side length b of the

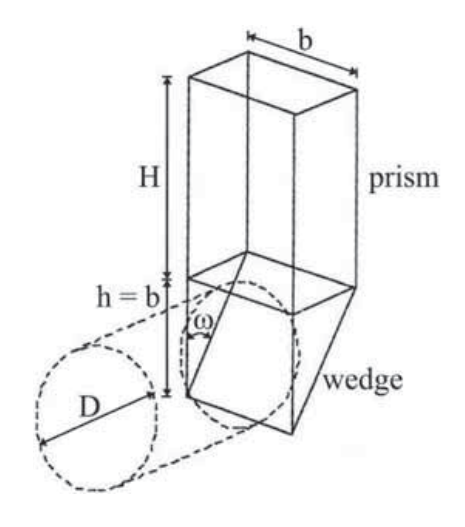


Figure 1. Failure mechanism (Horn 1961).

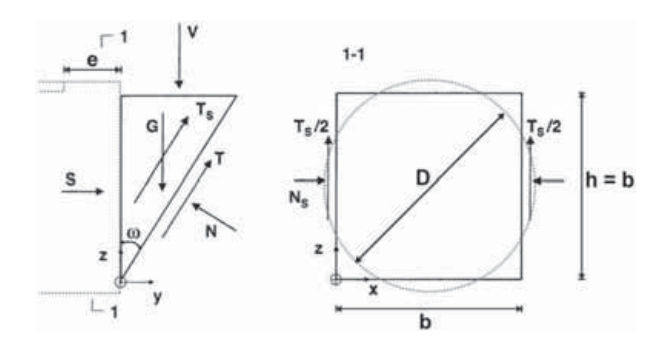


Figure 2. Loading and forces acting on the wedge after Anagnostou & Kovári (1994).

square is obtained by setting its area equal to that of the circular tunnel face:

$$b = D\frac{\sqrt{\pi}}{2}. (1)$$

By neglecting the horizontal shear force at the wedge—prism interface we obtain from the equilibrium conditions of the wedge:

$$S = \frac{V + G}{\tan(\omega + \phi)} - \frac{T_s}{\cos\omega(\tan\omega + \tan\phi)},$$
 (2)

where G, V and  $T_s$  denote the own weight of the wedge, the force resulting from the overlying prism and the frictional resistance at the two lateral slip surfaces, respectively. The weight.

$$G = \gamma \frac{1}{2} b^3 \tan \omega, \tag{3}$$

where  $\gamma$  is the unit weight of the soil, while the load V exerted by the prism is calculated by applying the silo theory to an extended prism comprising the unsupported span e:

$$V = \sigma_{\rm silo} b \left( e + b \tan \omega \right) \tag{4}$$

where the silo pressure.

$$\sigma_{\rm silo} = \frac{r \, \gamma}{\lambda \, \tan \phi} \left( 1 - e^{-\lambda \, \tan \phi \frac{H}{r}} \right) \tag{5}$$

and

$$r = \frac{b/2}{\frac{1}{\tan \omega + e/b} + 1}.$$
 (6)

The symbol  $\lambda$  appearing in Equation 5 denotes the ratio of horizontal to vertical stress, which in silo

theory is assumed to be constant (the coefficient of lateral stress). According to Equations 4 and 5, the unsupported span e between the tunnel face and the tunnel lining increases the prism volume and therefore the resulting force V on the wedge.

Following Anagnostou & Kovári (1994), the frictional resistance.

$$T_{s} = \tan\phi \ \lambda_{w} \ b^{2} \tan\omega \left( \frac{2\sigma_{silo}}{3} \left( 1 + \frac{e}{b \tan\omega} \right) + \frac{b\gamma}{3} \right), \tag{7}$$

where  $\lambda_{w}$  is the coefficient of lateral stress for the wedge. The coefficients of lateral stress  $\lambda$  for the prism and  $\lambda_{w}$  for the wedge are chosen according to Anagnostou & Kovári (1994) to be 0.80 and 0.40, respectively. The critical opening angle  $\omega$  of the wedge (angle of the inclined slip plane to the vertical) is determined iteratively so that the necessary support force S becomes maximum. As can be seen by means of a dimensional analysis, the computational results may be presented in the following way:

$$\frac{s}{\gamma D} = f\left(\frac{H}{D}, \frac{e}{D}, \phi\right),\tag{8}$$

$$\omega_{\text{crit}} = f\left(\frac{H}{D}, \frac{e}{D}, \phi\right),$$
 (9)

where *s* denotes the necessary support pressure. Figures 3 and 4 contain the graphical representation of these two equations for an angle of internal friction of 33° (the value of the sand used in the physical models).

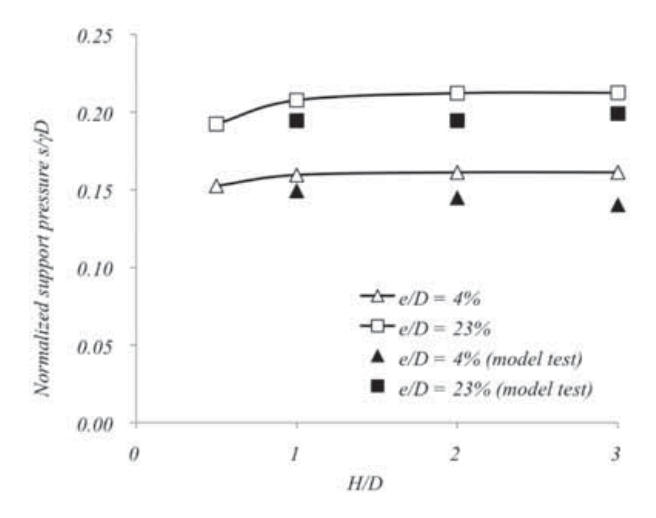


Figure 3. Required support pressure s (normalized by  $\gamma D$ ) in the function of the cover to diameter ratio H/D (angle of internal friction  $\phi = 33^{\circ}$ ).

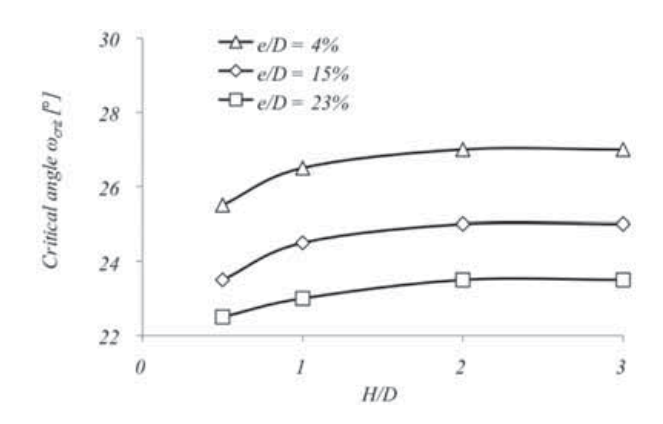


Figure 4. Critical opening angle  $\omega$  in function of the cover to diameter ratio H/D (angle of internal friction  $\phi = 33^{\circ}$ ).

#### 3 EXPERIMENTS

#### 3.1 Physical model

The model consists of a sand box with inner dimensions of height × length × width = 960 mm × 920 mm × 150 mm (Figure 5). In order to reduce friction and also to visualize clearly the soil movements, the front and rear plate of the box container are made of glass. The friction angle between glass and sand was measured to be 9° (coefficient of friction  $\mu$  = 0.16). A transparent sheet with a millimetre grid was fixed on the front glass plate in order to monitor soil movements with a higher accuracy.

The tunnel lining was modelled by a clear acrylic (PMMA) half pipe with an inner diameter of 130 mm (Figure 6). The half pipe tunnel model was positioned against the front glass plate of the box to obtain symmetry conditions. The width of the sand box (150 mm, i.e. about 2.5 times the tunnel radius) allowed the failure mechanism to develop fully without interference from the rear side of the box.

The tunnel face support was modelled in two ways: (i) by a rigid movable face with a 25 mm thick PVC plate and, (ii), as a flexible face by using a pressurised air bag made from latex (0.15 mm thick). Due to the abrasiveness of the quartz sand, it was not possible to use a thinner latex membrane.

The model was filled with uniform fine sand (grain size  $D_{max} = 0.3$  mm, void ratio = 0.577,  $\varphi = 33^{\circ}$ ,  $\gamma = 17$  kN/m³). The sand was built up in layers of 40 mm. Each layer was manually compacted with a wooden plate and then a fine marker line of black electrocorundum (grain size 0.5–0.8 mm) was placed at the front glass plate in order to visualize the deformations better and to detect the start-point of any failures. The marker line

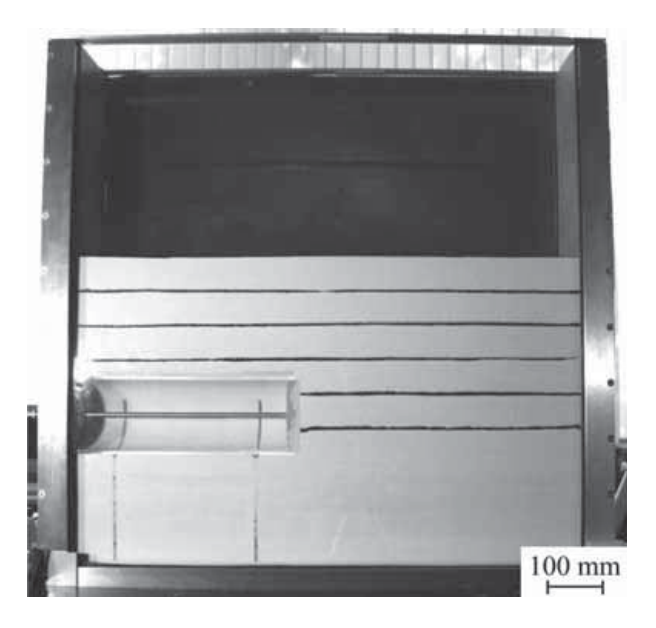


Figure 5. Model with rigid face with built up sand layers.

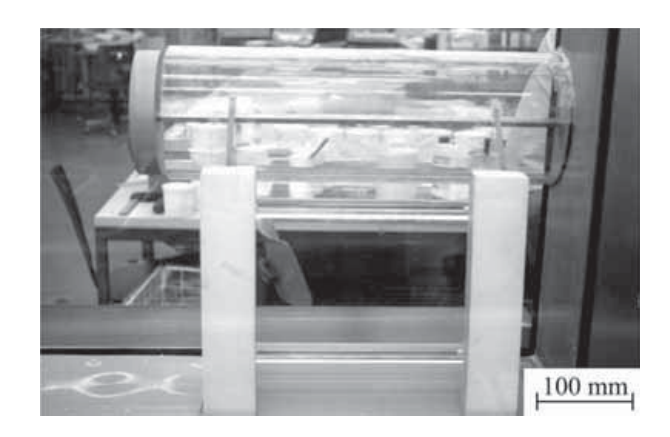


Figure 6. Tunnel model (seen from the rear glass plate).

(Figure 7) was fine enough not to influence the failure kinematics. A certain non-uniformity of the void ratio beneath the tunnel is of minor importance for the failure mechanism.

Soil movements were monitored optically by means of the millimetre grid. In order to measure the required support pressure at this scale a special manometer was developed. The pressurised air bag was connected by a plastic hose to the manometer. On a mm-scale the excess pressure in the air bag could be directly determined by measuring the difference between the water column connected to the pressurised air bag and the water column (WC) connected to atmospheric pressure (Figure 8). It is possible to achieve an accuracy of about ±2 mm WC with this liquid pressure measurement system.

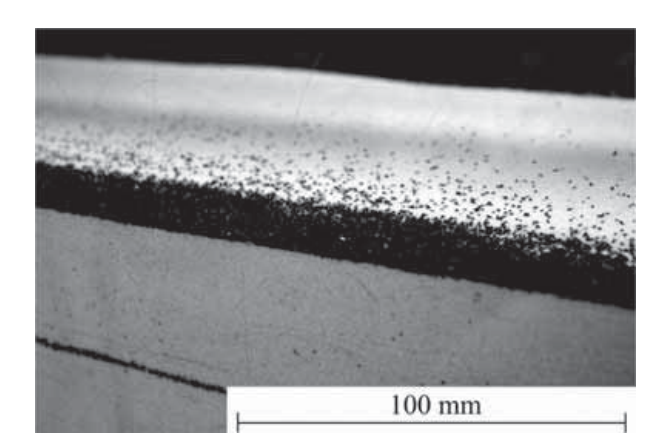


Figure 7. Marker line of black electrocorundum.

Table 1. Performed tests and varied parameters.

Tunnel face type	H	H/D	e	e/D
	[mm]	[-]	[mm]	[-]
Rigid movable face	130	1	20	0.15
	260	2	20	0.15
	390	3	20	0.15
Flexible face	130	1	5	0.04
	260	2	5	0.04
	390	3	5	0.04
	130	1	30	0.23
	260	2	30	0.23
	390	3	30	0.23

## 3.2 Performed tests

In order to investigate the influence of the overburden and of the unsupported span on the failure mechanism and on the required support pressure a total of nine tests were carried out (Table 1).

In the case of a rigid face, only the overburden H was varied (between D and 3D), while the so called unsupported span e (i.e. the distance between the rigid lining and the face) was chosen to be equal to 20 mm (i.e., 0.15 D).

Using the pressurised air bag, six tests were performed with the same cover to diameter ratios as with the PVC plate. The tests have been carried out for two different values of unsupported span.

# 3.3 Rigid movable face

In order to take the unsupported span into account, the PVC plate simulating the rigid face support was positioned prior to the test so that it exceeded the acrylic half pipe by 20 mm. This procedure also prevented the formation of a void at the tunnel crown. The pole fixed to the centre of gravity of the PVC plate was then blocked in order to prevent it moving whilst building up the sand layers. Before starting the test, the pole was released. The pole was then pulled back in steps of about 2.5 mm

into the tunnel. After every step a photograph was taken for later evaluation on the computer screen. The kinematics of the failure mechanism were evaluated in this series of tests.

The tunnel face pressure was not monitored in these tests. At this scale it would be difficult to build earth pressure cells into the tunnel face model. In addition to that, the accuracy of small earth pressure cells would probably be insufficient.

### 3.4 Flexible face

After positioning the air bag in the tunnel model with the chosen unsupported span, the air bag was blown up through the middle valve of the manometer (Figure 8) to a pressure higher than the estimated required support pressure. The middle valve was then closed and the sand layers were built up. The sand around the tunnel crown was carefully compacted in order to avoid larger deformations of the air bag. Due to the very low stiffness of the latex air bag, small movements of the sand at the tunnel crown cannot be avoided. A thicker air bag would have influenced the kinematics of the failure mechanism and consequently the required support pressure as well.

After building up the sand layers, the top and bottom valve were slowly opened in order to lower the air pressure in the bag. This was done in small



Figure 8. Manometer with 3 valves.

steps of about 2 mm WC. Photographs after every step were taken. The start-point of a failure could be determined on the computer screen with greater accuracy and the associated support pressure read in mm WC on the mm-scale of the manometer. In order to avoid a falsification of the results, it is necessary to distinguish between local soil loosening phenomena and the start-point of the failure mechanism observed during the previously performed PVC plate tests.

#### 4 TEST RESULTS

#### 4.1 Rigid movable face support plate

Figure 9 shows five stages of such a test. The variable *x* denotes the distance of the PVC plate from the front boundary of the acrylic half pipe. At the beginning of the test (Stage 1), the distance *x* is equal to the unsupported span (20 mm ahead of the face). Once the PVC plate is pulled back by 5 mm (about 4% of the tunnel diameter), the failure plane of the wedge is already well recognisable (Stage 2). In Stage 3 the failure body is completely developed (wedge and prism), i.e. the prism reaches the surface and surface settlement therefore begins

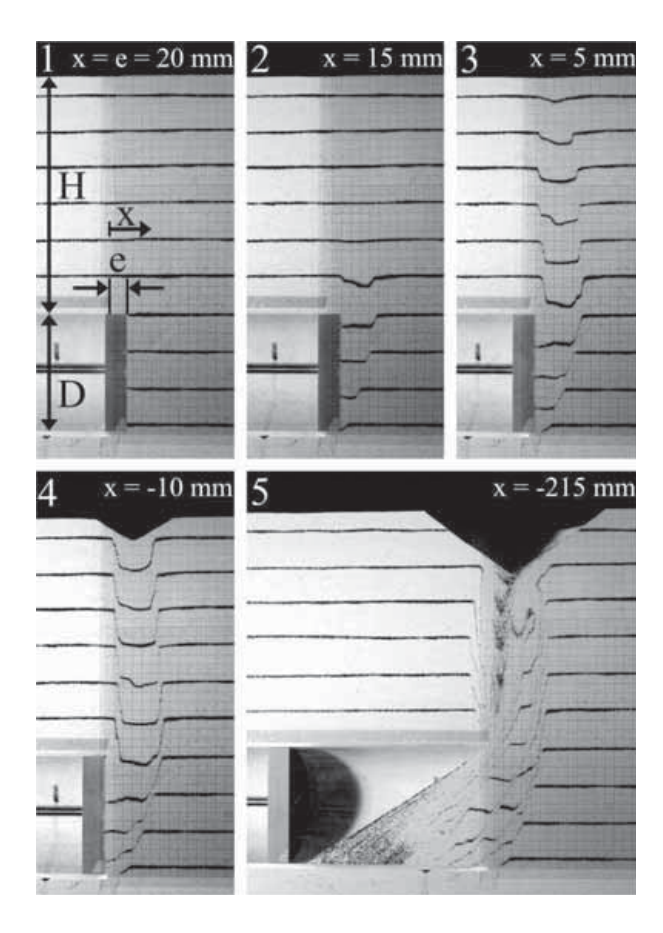


Figure 9. Observed failure mechanism (H/D = 2, e/D = 15%).

to appear. The propagating failure mechanism then results in a crater at the surface (Stage 4). The final state of equilibrium is shown in Stage 5. The crater at the surface was also observed at an overburden of three times the tunnel diameter.

The average critical opening angle  $\omega$  of the wedge of the three tests was measured to be 22°, which agrees well with the calculated value of 25° (Figure 4).

#### 4.2 Flexible face

Figure 10 shows four stages of a flexible face test. The initial state before starting the test is displayed in Figure 10a. It was observed that the failure mechanism sets in suddenly (Figure 10b) while the pressure in the air bag is slowly being lowered. Subsequently, and without any significant further lowering of the pressure in the air bag, the collapse of the tunnel heading continues (Figure 10c) until a new state of equilibrium is reached (Figure 10d).

Even though the stiffness of the latex membrane is very low, the base of the air bag prevents the wedge from slipping into the tunnel on the tunnel floor. The failure body is therefore slightly shifted upwards. It must be pointed out that the chosen unsupported span of 23% D as shown in Figure 10 is unrealistically high. At a smaller unsupported span of 0.04 times the tunnel diameter, the resulting failure body was closer to the one observed in the rigid face tests.

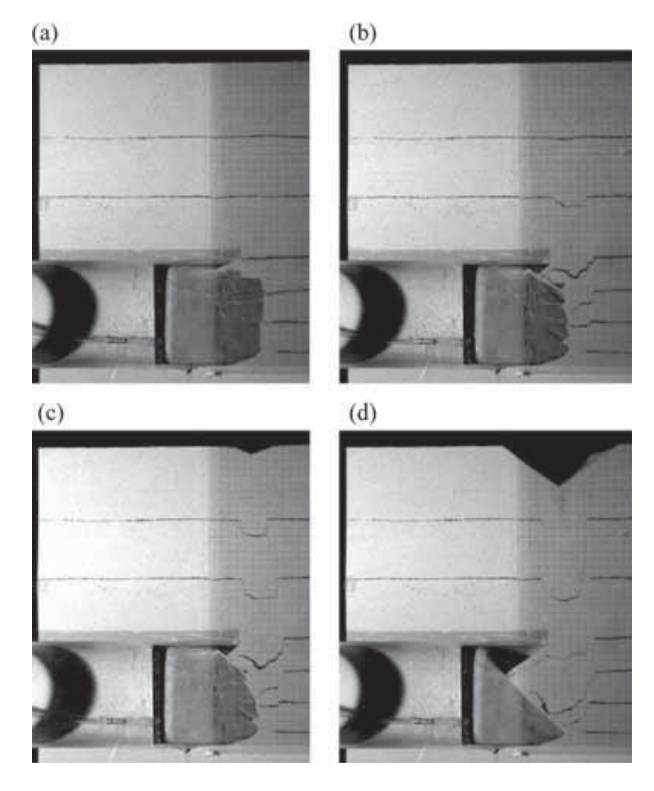


Figure 10. Flexible face test (H/D = 2, e/D = 23%): (a) initial state; (b), (c), (d) sudden failure.

Figure 3 compares the experimental with the computational results. The average required support pressure was measured at 32 and 43 mm WC for an unsupported span to diameter ratio of 4% and 23%, respectively. These values are about 10% lower than the predictions from the limit equilibrium model (36 and 47 mm WC, respectively). By correcting the measured values to take account of the frictional forces between sand and the front glass plate, it was possible to reduce the difference to 2% (Messerli, 2007). Other reasons for the difference between experiment and calculation include the pressure acting upon the crown (the crown is actually supported in the physical model) and the simplification of not taking account of the effect of the horizontal shear stress at the prism—wedge interface. It should be noted, furthermore, that the accuracy of the manometer amounts to approximately 5% ( $\pm 2$  mm).

For the investigated ratios of overburden to diameter  $(1 \le H/D \le 3)$ , no significant dependency of support pressure to overburden could be observed. This observation has also been made in other research works (e.g., Kirsch 2009) and can be reproduced computationally (Fig. 3).

#### 5 CONCLUSIONS

The experiments described above are adequate for modelling tunnel face collapse. The selected material, the chosen dimensions and the use of symmetry conditions reduced to an acceptable level the boundary effects on the failure mechanism. The pressure measurement system operated with good levels of accuracy for the very low pressures during the test procedure.

The test results agree well with the limit equilibrium calculations with respect both to the kinematics of failure and to the required support pressure. The rigid face test enabled a clear visualisation of the failure mechanism and confirmed the failure mechanism proposed by Horn (1961). The difference between the measured and the calculated required support pressure lies within the range of accuracy of measurement.

## REFERENCES

- Anagnostou, G. & Kovári, K. 1994. The Face Stability of Slurry-shield-driven Tunnels. *Tunnelling and Underground Space Technology* 9: 165–174.
- Horn, M. 1961. Horizontaler Erddruck auf senkrechte Abschlussflächen von Tunneln. Landeskonferenz der ungarischen Tiefbauindustrie, Budapest (German translation, STUVA, Düsseldorf).
- Kirsch, A. 2009. Experimental and Numerical Investigation of the Face Stability of Shallow Tunnels in Sand. ITA-AITES World Tunnel Congress "Safe Tunnelling For The City and Environment", Budapest.
- Meguid, M.A., Saada, O., Nunes, M.A. & Mattar, J. 2008. Physical modelling of tunnels in soft ground: A review. *Tunnelling and Underground Space Technology* 23: 185–198.
- Messerli, J. 2007. Modellversuche zur Stabilität der Ortsbrust oberflächennaher Tunnels. BSc Thesis, ETH Zurich.
- Vardoulakis, P., Stavropoulou, M. & Exadaktylos, G. 2009. Sandbox modeling of the shallow tunnel face collapse. Rivista di Geotecnica 1/2009, 9–21.
- Vermeer, P.A., Ruse, N. & Marcher, Th. 2002. Tunnel Heading Stability in Drained Ground. Felsbau, 8–18.